Innovative Silicon Compatible Materials for Light Emitting Devices

Adriana Scarangella[1], Riccardo Reitano[2], Francesco Priolo[1, 2, 3], Maria Miritello[1]*

[1]*CNR IMM, Via S. Sofia 64, Catania 95123, Italy*
[2]*Dipartimento di Fisica e Astronomia, Università di Catania, Via S. Sofia 64, Catania 95123, Italy*
[3]*Scuola Superiore di Catania, Università di Catania, Via Valdisavoia 9, Catania 95123, Italy*

*Corresponding author: E-mail: maria.miritello@ct.infn.it

Abstract

The paper reports the potentialities of innovative silicon compatible materials for light emitting devices. In particular thin films of Er doped yttrium oxide have been synthesized by a technique totally compatible with ULSI processes. Through the structural characterization, we will verify the high stability of the film and the good dopant dissolution. Moreover, by the investigation of the optical properties, we will demonstrate that the use of this compound is effective to introduce more than 10^{21} Er/cm^3 in optically active state, value that cannot be reached in other Si compatible materials. The influence of Er content on the optical properties will be described in details. Moreover, we will propose the introduction of a proper sensitizer for Er, bismuth, in the same thin film. In particular, we will show that the (Er+Bi) co-doped yttrium oxide is a perfect host to overcome another important drawback of Er doped materials that is its low absorption cross section. The influence of Bi and Er contents on optical properties will be extensively discussed along the paper. Through the optimization of ratio between Bi and Er concentrations, high energy transfer efficiency will be reached with simultaneously a consistent increase of the effective Er cross section. A factor of more than three orders of magnitude have been obtained with respect to the direct excitation of Er. Copyright © VBRI Press.

Keywords: Light emitting devices, erbium, yttrium oxide.

Introduction

In the last decades, the limitations reached by silicon microelectronics brought the scientific community to move towards the field of silicon photonics with the aim to use photons instead of electrons for carrying and processing information inside a Si chip [1, 2]. Among the investigated optically active Si-compatible media, erbium-based materials have been extensively studied since Er de-excitation, from $^4I_{13/2}$ to $^4I_{15/2}$ level, involves the emission of a photon at 1.54 μm that corresponds to a minimum loss of silica optical fibers [1-3]. However, its excitation cross section of about 10^{-21} cm^2 [4] is a limiting factor to achieve high optical efficiency, and at the same time introducing a high number of Er ions in Si-compatible materials is still challenging owing to low Er solid solubility [5]. To overcome these limits, successful approaches have been recently pursued. The first one concerns the development of mixed rare earth (RE) oxides or silicates, where Er-based materials have been employed [7-11]. Here it is possible to control in a continuous way the Er content up to 10^{22} Er/cm^3, without cluster formation and also by limiting detrimental Er-Er interactions such as concentration quenching [12-14]. Among all the mixed RE compounds, yttrium oxide is a good candidate as host for Er, owing to its comparable crystalline structure

with respect to one of Er oxide and to the similar Er and Y ionic radii. Moreover, Y^{3+} is not optically active, thus giving transparency properties to its compound from the visible to the infrared (IR) range and permitting to assign all the material's optical properties to Er ions. In addition, thanks to the development of complementary metal-oxide-semiconductor (C-MOS) compatible synthesis techniques, it is possible to realize good quality thin films with high thermal stability on silicon [15]. Thus, Er doped yttrium oxides have reached great attention for the realization of CMOS-compatible Si-based light sources operating at room temperature (RT). The second strategy to further increase the Er optical efficiency in Si-compatible materials is to enhance the low Er excitation cross section, with the introduction of a proper sensitizer that can absorb and transfer the energy more efficiently than Er ions. Successful results have been reached by the development of luminescent Si nanostructures, such as Si nanowires [16] and Er-coupled Si nanoclusters [1, 17], that have been demonstrated to be optically efficient both under optical and electrical pumping at RT. However up to now the reached efficiency is still not enough for commercial devices. Despite other REs have been already proposed as Er sensitizers, such as Yb^{3+} [18], recently the use of optically active metal ions, such as bismuth, as REs sensitizer emitting in the

visible wavelength range is reported [**19-21**]. However, very few papers report the occurrence of energy transfer (ET) between Bi and Er ions [**22-25**].

In this paper we propose the use of both approaches, i.e. the Er doped yttrium oxide thin films to dissolve high concentrations of active centers in a Si compatible host and at the same time the introduction of Bi as an Er sensitizer as a suitable material for light emission. The structural and optical properties of Er and Bi co-doped yttrium oxide thin films will be discussed, by focusing on the dependence by the Er and Bi concentrations. The stability of the films and the dopants dissolution in the host will be analyzed. Moreover, we will treat the coupling of Er and Bi by investigating the best Er and Bi ratio to maximize the optical efficiency of the system.

Experimental

Material synthesis

Er doped Y_2O_3 thin films were deposited by AJA UHV magnetron co-sputtering (base pressure 10^{-9} mbar). All the depositions have been performed in argon atmosphere (5×10^{-3} mbar) by radio frequency co-sputtering of two targets (Y_2O_3 and Er_2O_3) on c-Si(100) substrates heated at 400 °C. The power applied to the Y_2O_3 target was fixed at 500 W, while that one to the Er_2O_3 target was varied between 25 W and 40 W. Some samples have been implanted with Bi ions at 270 keV, the energy has been chosen in order to locate the Bi distribution almost in the center of the films thickness, as calculated by Stopping and Range of Ions in Matter (SRIM) simulations [**26**].

Both the Er doped and (Er+Bi) co-doped samples have then be annealed at 800 °C for 30 min in oxygen atmosphere to stabilize the Bi^{3+} and Er^{3+} oxidation state and to remove eventual defects left over by the implantation process.

Characterizations

The films stoichiometry, elemental concentration and thickness have been evaluated by Rutherford Back-Scattering Spectrometry (RBS). RBS measurements have been performed by using a 2 MeV energy He^+ beam with the detection at an angle of 165° with respect to the beam direction.

The crystalline structure of the samples has been studied by X-Ray Diffraction (XRD) analyses performed with a Bruker-AXSD5005 diffractometer by using Cu Kα radiation with a grazing incidence angle of 1.0° and the detection angle 2θ varied between 18° and 60°.

The optical properties of all the annealed films have been analyzed by photoluminescence (PL) measurements at room temperature. The 488 nm line of an Ar laser was chosen because in resonance with the $^4I_{15/2} \rightarrow {}^4F_{7/2}$ Er^{3+} transition, while the 325 nm line of an He-Cd laser was chosen as pumping source, because it could permit to excite the UV band of all the possible Bi oxidation states. In both cases, the laser beam was

chopped through an acousto-optic modulator with a frequency of 11Hz. PL signals have been recorded by a three gratings monochromator and a lock-in system modulated at the same chopping frequency. The PL spectra were analyzed in the range between 400 nm and 1700 nm thanks to water cooled photomultiplier and a liquid nitrogen-cooled Ge detector. Time resolved PL measurements were performed by detecting the modulated PL signal with a Hamamatsu photomultiplier tube and then by analyzing the signal with a photon counting multichannel scaler. The overall time resolution of the system is 30 ns.

Results and discussion

Structural properties

In this section we report the structural properties of the Er and (Er+Bi) co-doped yttrium oxide thin films. First of all, the stoichiometry of the films and the elemental concentration of both the dopants, Er and Bi, have been evaluated by RBS measurements. **Fig. 1** reports the RBS spectra of the two annealed Er doped Y_2O_3 oxide thin films synthesized with the same power supplied to the Y_2O_3 target and different powers applied to the Er_2O_3 target, in particular 25 W and 40 W.
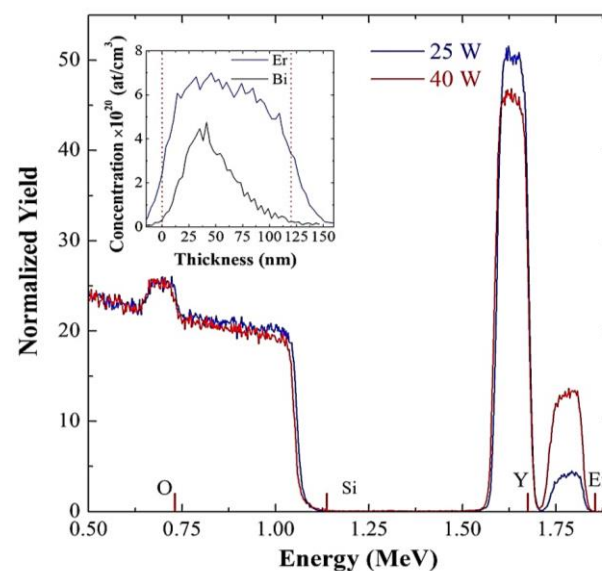

Fig. 1. RBS spectra of Er doped Y_2O_3 thin films on c-Si for different powers applied to the Er_2O_3 target. The threshold energies of O, Si, Y, and Er are also indicated. In the insert the Bi and Er depth distribution profile in (Er+Bi) co-doped Y_2O_3 for higher Er and Bi contents.

Four signals are distinguishable, that can be identified as the depth profiles of O, Si, Y, and Er, as indicated by the threshold energies of the respective elements. For both samples the Si signal is relative to the silicon substrate, while all the other signals are relative to the thin film. All the signals appear constant along all the film thickness, thus demonstrating a uniform chemical composition. By simulating the RBS curves with the software SIMNRA 6.0 [**27**], the film stoichiometry was verified to be (Y+Er):O = 2: 3, and the Er content has been evaluated as 1.1 Er% and 3.3

Er% respectively for powers applied to the Er_2O_3 target of 25 W and 40 W. The Er profile can be plotted, by converting the normalized yield and the energy axes, respectively, in volume concentration and depth scales. In particular, for the higher Er content the Er depth profile has been reported in the insert of **Fig. 1**. A constant Er concentration of about 7×10^{20} Er/cm^3 has been estimated along all the film thickness of 120 nm, while a value of 3.0×10^{20} Er/cm^3 for the lower power applied to the Er_2O_3 target.

When Bi is introduced in the two films, the Bi signal is partially overlapped with the Er one, since the energy thresholds are 1.855 MeV and 1.820 MeV, respectively for Bi and Er [28, 29]. Therefore, we have used as reference sample a Bi doped Y_2O_3 thin film implanted with the same dose and energy used for the samples under investigation. The obtained Bi profile has been reported in the insert of **Fig. 1** for the case of higher Bi doping. It has the typical Gaussian shape related to the ion implantation processes, and a Bi content of 2.8×10^{20} Bi/cm^3 and 7.0×10^{20} Bi/cm^3 has been evaluated for the two nominal implanted doses, corresponding to the 0.4 Bi% and 1.0 Bi% respectively.
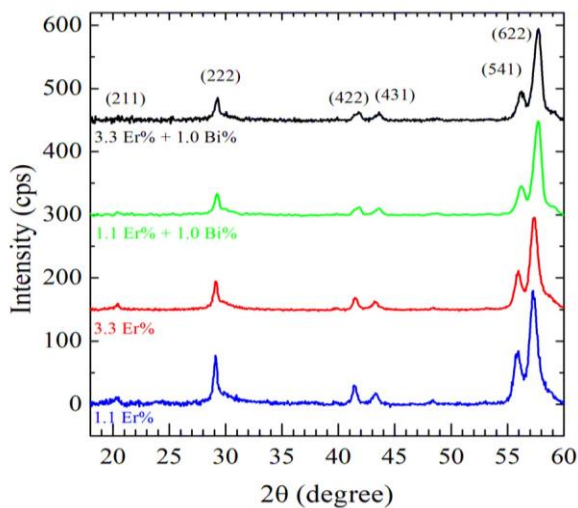

Fig. 2. XRD patterns of the Y_2O_3 thin films containing only Er and (Er+Bi) for the two used Er concentrations. The Miller indices corresponding to the Y_2O_3 bulk are also indicated [**30**].

In order to study the influence of Er and Bi incorporation in the Y_2O_3 crystalline structure, XRD analyses have been performed in glancing configuration. The XRD spectra of both Er-doped Y_2O_3 and (Bi+Er) co-doped Y_2O_3 thin films for the higher Bi content, 1.0 Bi%, are shown in **Fig. 2**. All the spectra appear very similar, independently of the Er content and Bi presence. In particular they are characterized by several intense peaks, which can be all associated to the polycrystalline body centered cubic structure of Y_2O_3 [**30**]: The Miller indices of the corresponding lattice planes are reported in the same figure. Other additional peaks associable to the formation of other crystalline phases are absent, thus confirming the good dissolution of both dopants inside the Y_2O_3 crystalline structure. Only a slight shift of the peaks towards higher angles is

observed, when Bi is introduced, and it was correlated to a slight shrinkage of the lattice parameter due to the larger ionic radius of Bi with respect to Y (1.03 Å and 0.9 Å respectively for Bi and Y). Thus, we can support the assert that both Er and Bi can replace Y in substitutional positions in the Y_2O_3 lattice.
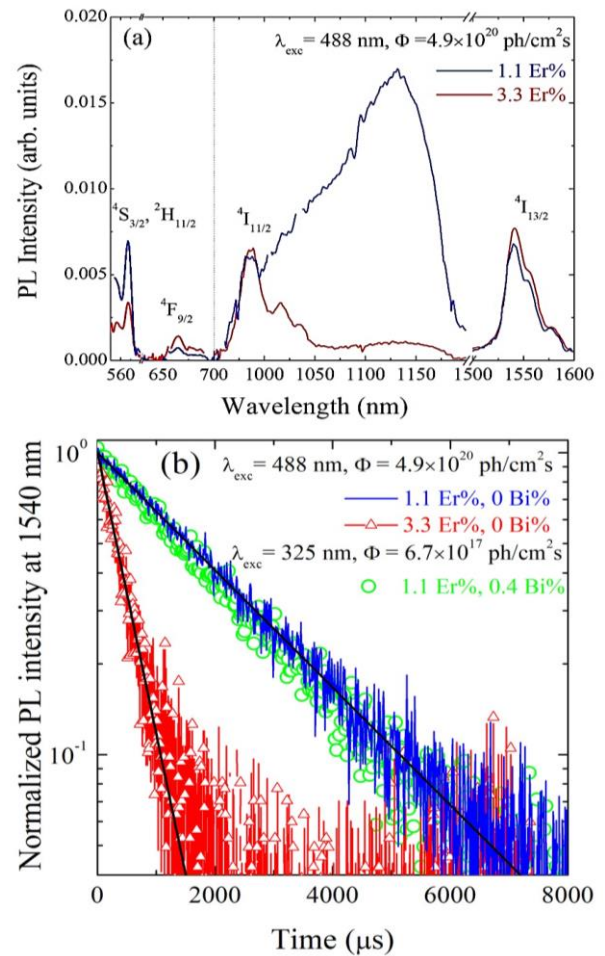

Fig. 3. (a) PL spectra over all the visible and IR range of the Er doped Y_2O_3 thin films, for the two Er contents. The measurements have been done under 488 nm and pump flux of 4.9×10^{20} ph/cm^2s. The Er excited levels involved for each peak PL emission are also indicated. (b) The relative time-resolved PL recorded at 1540 nm have been reported. In comparison also the decay curve recorded under 325 nm and pump flux of 6.7×10^{17} ph/cm^2s has been plotted. The exponential fits have been also reported.

Optical properties

Visible and IR emission

The optical properties of all the annealed films have been analysed by PL and lifetime measurements at RT.

We have firstly analyzed the Er-doped Y_3O_3 thin films by using the 488 nm line of an Argon laser as pumping source, with a photon flux of 4.9×10^{20} ph/cm^2s. This excitation wavelength permits to excite directly the $^4I_{15/2} \rightarrow {}^4F_{7/2}$ Er^{3+} transition. The PL spectra obtained for 1.1 Er % and 3.3 Er% have been shown in **Fig. 3 (a)**: different emission peaks are detected in the visible and IR region, in particular centred at 566 nm, 660 nm, 980 nm and 1540 nm, that correspond

respectively to the Er^{3+} transitions from ($^4S_{3/2}$, $^2H_{11/2}$), $^4F_{9/2}$, $^4I_{11/2}$ and $^4I_{13/2}$ to the $^4I_{15/2}$ ground state. The additional broad emission peaked at 1140 nm is not ascribed to Er emission but rather to the Si band edge emission from the oxidized silicon interface, that typically can be formed. The presence of all the radiative emission peaks is made possible by the long radiative lifetimes that characterize the Y_2O_3 host [**14**.

By the comparison of the two samples, we can observe an increase of PL at 566 nm and a simultaneous decrease of PL at 660 nm by increasing Er content. The reduction of the green emission despite the increase of the Er emitting centers can be justified by a corresponding increase of the nonradiative decay rate of the $^4S_{3/2}$ level, owing to the occurrence of the cross relaxation (CR) $^4S_{3/2}+^4I_{15/2}\rightarrow^4I_{9/2}+^4I_{13/2}$ [**14**]. Since the CR mechanism is an energy transfer process between one excited Er ion and another one in the ground state, it becomes more probable by reducing the Er–Er distance, i.e. by increasing the Er content [**14**].

Instead, in the IR range, we observe similar PL intensities both at 980 nm and 1540 nm for both samples, despite the 3-fold increase of Er content. In order to explain it, we have acquired also the decay times of the PL at 1540 nm that have been reported in **Fig. 3 (b)** for both the Er concentrations. Both curves have a single exponential decay, thus by proper fits, values of 2.2 ms and 0.5 ms have been found respectively for 1.1 Er% and 3.3 Er%. The observed reduction of the Er lifetimes at 1540 nm with increasing the Er concentration may be explained by the occurrence of up conversion (UC) phenomena, well known in Er-doped systems [**11, 12**]. The UC mechanism consists in resonant energy transfer between excited Er ions, $^4I_{13/2}+^4I_{11/2}\rightarrow^4I_{15/2}+^4F_{9/2}$. By increasing the Er ions during the light travel through the host the probability that the energy can be lost to impurities, such as -OH centers, increases [**5, 12, 32**], by dissipating it non-radiatively. Thus, the reduction of lifetime, by a factor of 4, justifies the presence of similar PL values at 1540 nm, despite the Er concentration increase from 1.1% to 3.3%.

The introduction of Bi in the Er doped Y_2O_3 does not induce any modification in the PL spectra and also the intensities are unchanged with respect to the $Er:Y_2O_3$ case when the system is excited under 488 nm. Instead if we choose the 325 nm excitation wavelength, that can involve the $^1S_0 \rightarrow {}^3P_1$ transition of Bi^{3+} ions as reported in [**33-35**], we observe PL emission from Er ions though this excitation wavelength is out of resonance of any Er energy levels. **Fig. 4 (a)** reports the PL spectra of (Er+Bi) co-doped samples under 325 nm for both the Er and Bi contents. The used photon flux is 6.7×10^{17} ph/cm^2s that is almost three orders of magnitude lower than the one used under 488 nm excitation.

For all the (Er+Bi) co-doped samples, all the peaks associable to the Er transitions have been detected, but with much higher intensities, about three orders of magnitude, with respect to the case of Er-doped films under resonant excitation, if normalized for the used pump fluxes. Moreover, in the visible range a further broad band appears overlapped to the Er peaks. The origin of this band can be associated to PL emission from the Bi ions that are not coupled with Er ones. In particular it can be ascribed to the optical transition between the excited state $^3P_1$ to the ground state $^1S_0$ [**36-38**], as depicted in the schema reported in **Fig. 4 (b)**. However, the Bi PL emission intensity is strongly decreased compared with the one from similar samples that contain only Bi and not Er, used as references (not shown). Therefore the simultaneous reduction of the Bi PL intensities and the appearance of all the typical Er emission peaks suggest the occurrence of efficient ET mechanisms from Bi to Er ions, owing to the already demonstrated good overlap between the excitation band of Bi ions in $Bi:Y_2O_3$ and of Er ions in $Bi+Er:Y_2O_3$ [**39, 41**] as depicted in **Fig. 4 (b)**. The higher Er PL intensities have been reached for 1.1 Er% and 1.0 Bi%.
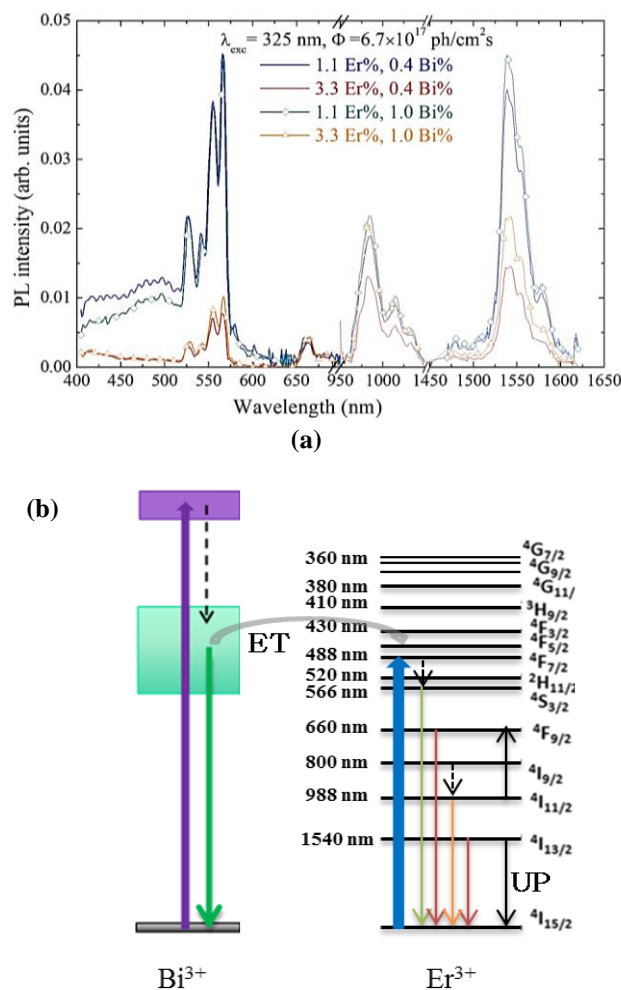

(a)

Fig. 4. (a) PL spectra over all the visible and IR range of (Er+Bi) co-doped samples under 325 nm excitation and pump flux of 6.7×10^{17} ph/cm^2s, by varying the Er and Bi concentrations. (b) Er and Bi energy levels schema reporting the most important optical transitions, i.e. Bi excitation under 325 nm wavelength, Bi radiative and non-radiative (ET) de-excitation, direct Er excitation under 488 nm wavelength, Er radiative emissions and UP (6).

To further unveil the efficiency of the ET process, we have verified that the presence of Bi does not influence the Er lifetime for all the involved emission peaks and for all the investigated Bi and Er concentrations. In **Fig. 3 (b)** we compare the Er decay time at 1540 nm for the case of 1.1 Er% and 0.4 Bi% observed under 325 nm excitation with the one from Er doped sample, containing the same Er content, observed under resonant excitation. The curves appear clearly unchanged. It means that Bi ions do not introduce any further non-radiative channels to Er de-excitation, and the energy transfer between Bi and Er involve only excitation to higher Er energetic levels.

About the dependence of ET efficiency on the Bi content, we can observe that for the lower Er concentration, 1.1 Er%, the Er related PL emissions increases slightly, about a factor 1.1, by increasing the Bi content from 0.4 Bi% to 1.0 Bi%, and a weak Bi PL emission at 500 nm is observable for both Bi concentrations. Instead, for 3.3 Er%, the Er related PL intensities increase by a factor of 1.6 by increasing Bi concentration and the Bi PL emission almost disappears. This suggest that for 1.1 Er% the optimized Er-Bi coupling is reached for the higher Bi content, corresponding to a Er:Bi ratio of almost 2:1: thus increasing further the sensitizers concentration is not beneficial. Instead if we consider the sample containing 3.3 Er%, the almost disappearance of Bi PL emission suggests that all the Bi ions introduced in the host transfer their energy non-radiatively to Er ions for both Bi concentrations. Therefore as confirmed by the enhancement of the Er related PL intensities by increasing Bi content, from Er:Bi of 8:1 to 3:1, the number of Er ions coupled with Bi is increasing.

A quantitative estimation of the ET efficiency can be done by considering the reduction of PL emission at 500 nm from Bi in absence of Er (in the Bi doped Y_2O_3 thin film), PL_{Bi}, with respect to the case of (Er+Bi) co-presence (in the (Er+Bi) co-doped Y_2O_3). PL_{Bi+Er}, for a fixed Bi content [**42**]. The formula is

$$\eta_{ET} = 1 - \frac{PL_{Bi+Er}}{PL_{Bi}} \qquad (1)$$

A value of about 70% and 98% have been estimated for 1.1 Er% and 3.3 Er% respectively.

Dependence of optical properties on pump flux

In order to investigate the potentiality of this system in light emitting devices or optical amplifiers at 1540 nm, we have investigated the dependence of optical properties on excitation pump flux, Φ. Indeed in Er-doped materials, the Er PL intensity at 1540 nm is typically limited at higher pump power by UC phenomena, as schematized in **Fig. 4 (b)**, especially by the so called first order upconversion (UC1), that involves the following mechanism $^4I_{13/2} + ^4I_{13/2} \rightarrow ^4I_{15/2} + ^4I_{9/2}$. The occurrence of these up-conversion processes in our samples has been investigated by studying the trend of the PL intensities as a function of the excitation flux, Φ. Both the direct (488nm) and mediated (325nm)
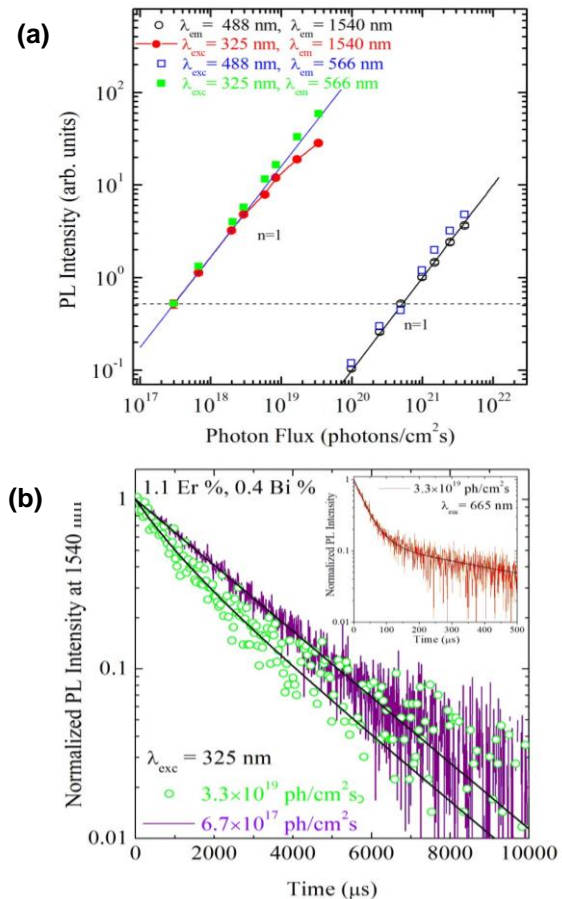

Fig. 5. (a) PL intensity versus photon flux recorded at 566 nm and at 1540 nm from (Er+Bi) co-doped Y_2O_3 under 325 (indirect) and 488nm (direct) excitation. Linear fits to the PL data are plotted. (b) Time-resolved PL recorded at 1540 nm under 325 nm at different pump fluxes. Insert: time-resolved PL measurement at 660 nm under higher pump fluxes at 325 nm.

(325 nm) excitation conditions have been considered: in particular the flux range was varied from 10^{19} ph/cm²s to 10^{21} ph/cm²s and from 10^{17} ph/cm²s to 10^{19} ph/cm²s, respectively for the 488 nm and 325 nm excitation wavelength. Owing to the similar PL behaviour of the (Er+Bi) co-doped Y_2O_3 samples containing different Er and Bi concentrations, from now on we will focus on the case of 1.1 Er% and 0.4 Bi% and we will use also the Bi doped Y_2O_3 thin film, as reference, in order to discern eventual influence coming from Bi ions. **Fig. 5 (a)** compares the PL trends of the green emission and the 1540 nm intensity as a function of Φ, both under 488 nm and 325 nm excitation. Even if not displayed in the figure, it is important to point out that the Bi PL emission in the Bi doped Y_2O_3 thin film increases linearly in all the investigated range. It means that the Bi emission is due to the absorption of only one photon in all the investigated flux range. To fit the trends of Er emission in (Er+Bi) co-doped Y_2O_3, the relation $I_{PL} \propto \Phi^n$, where n is the number of photons absorbed [**45**], was used. The fits are reported in the same figure as well. The same linear trend has been recorded for all the observed Er emission peaks in (Er+Bi) co-doped Y_2O_3 under 488 nm excitation. **Fig. 5 (a)** reports only

the trend of Er emission at 1540 nm (black empty dots) and at 566 nm (green full squares) as examples. Instead, under mediated excitation similar PL intensities have been reached for three orders of magnitude lower Φ. The PL emission peaked at 1540 nm follows a linear behaviour only for fluxes lower than 3×10^{18} ph/cm^{2}s ($n = 1$) and then it becomes sub-linear ($n<1$). It means that for higher fluxes the Er $^4I_{13/2}$ energy level is partially depleted by the occurrence of one or more upconversion mechanisms. However, the trend of the 566 nm emission preserves the linear behaviour, as can be seen in **Fig. 5 (a)** in the green squared curve, as well as the one concerning the 980nm emission (not shown).

The occurrence of UC1 is also confirmed by the decay curves as shown in **Fig. 5 (b)** that reports the lifetime recorded at 1540 nm for two different photon fluxes, 3×10^{17} ph/cm^{2}s (low excitation Φ, linear regime) and 3×10^{19} ph/cm^{2}s (high excitation Φ, sub-linear regime), under 325 nm excitation. At the higher excitation flux, the curve is characterized by a faster decay in the first instants, while a simple exponential decay is observed for the lower one. Both curves follow the same parallel decay for longer times. It suggests a depletion of the $^4I_{13/2}$ energy level due to up-conversion mechanisms. However, the decay times of the $^4S_{3/2}$ (emission at 566 nm) and of the $^4I_{11/2}$ (emission at 980 nm) energy levels (not shown) are not affected by the Φ, as expected by the linear trend of the respective PL intensities, thus excluding the occurrence of the up-conversion processes involving these levels [**14**]. Values of about 25 µs and 800 µs have been found for the 566 nm and 980 nm emissions, respectively, independently by the excitation conditions, and comparable with the values reported for similar systems [**14, 46**]. The only decay curve that changed in the high pumping regime is the one corresponding to the 660 nm emission. As it can be seen in the inset of **Fig. 5 (b)**, for high photon flux the lifetime shows two distinct components. The fastest one is independent of the Φ and has a value of about 38 µs, representing the characteristic lifetime of the $^4F_{9/2}$ energy level. The much slower component appears only for highest pump flux and it has a value of about 500 µs. It can be associated to the UP mechanism depicted in **Fig. 4 (b)** [**47**] that becomes more probable for higher excitation fluxes. It involves two neighbouring Er ions excited in the $^4I_{13/2}$ and $^4I_{11/2}$ energy levels, respectively. The energy emitted non-radiatively by the first one to reach the ground state can be absorbed by the second one, which is promoted to the $^4F_{9/2}$ level by an exchange of 3 phonons [**47**]. This explains also why the observed slow component in the decay time (0.5 ms) is comparable to the characteristic lifetime of the underlying $^4I_{11/2}$ level.

These results demonstrate that PL intensities both in the visible and IR range keep a linear trend for an extended range, up to 3×10^{18} ph/cm^{2}s, under 325 nm excitation.

Moreover, from the comparison of Er linear PL trends under resonant and mediated excitation, it is possible to observe that under mediated excitation we can reach similar PL intensities with respect to the direct excitation but with almost three orders of magnitude lower pump fluxes. Through the fit of these trends we have also estimated the effective excitation cross section in presence of Bi. Indeed in the linear regime, the PL intensity can be approximated by the relation [**5, 14**]

$$I_{PL} \propto \sigma\Phi\frac{\tau}{\tau_{rad}} \qquad (2)$$

where, τ is the total lifetime, τ_{rad} is the radiative lifetime, and σ is the Er effective excitation cross section. Since the measured τ does not change by varying the excitation condition (as shown in **Fig. 3 (b)**), the ratio of the slopes of the two PL trends at 1540 nm gives the ratio of the effective excitation cross sections under direct Er absorption, σ_{Er}, and under mediated excitation, σ_{Er+Bi}. From the data in **Fig. 5 (a)**, we found that σ_{Er+Bi} is about 2220 times higher than σ_{Er} [**39**]. Assuming σ_{Er} equal to 2.4×10^{-21} cm^2, we can estimate a σ_{Er+Bi} value of 5.3×10^{-18} cm^2, which is compatible with 10^{-17} cm^2, value reported for Bi^{3+} direct excitation cross section in BiGeO [**48**]. This is another confirmation of the very efficient energy transfer between Bi^{3+} and Er^{3+} ions in Y$_2$O$_3$ films; moreover, it is interesting to underline that this value is one of the highest obtained for Er in Si compatible hosts [**43, 44**].

Conclusion

In conclusion, we have demonstrated the great potentialities of (Er+Bi) co-doped thin film as silicon compatible light emitter both in the visible and IR region. The structural characterization and the PL measurements have been evidenced the good dopants dissolution and the optical activities of both dopants in this host. In particular the ET efficiency between Bi and Er have been evaluated and the best Er and Bi ratio have been found in order to maximize the PL emission in the visible and IR range. Also, the optical properties have been confirmed in an extended flux range. Finally, the effective Er excitation cross section by Bi ET have been estimated to be 2200 times higher than the direct excitation, by reaching the highest values observed in literature. These results make this material very promising as an efficient visible emitter and a Si-compatible optical amplifier at 1540 nm.

Author's contributions

A.S. realized the Bi-doped yttrium oxide thin films and performed all the structural and optical characterizations; she contributed to data interpretation and wrote the paper. R.R. supervised the optical characterization. F.P. contributed to supervise the experiments, the data interpretation and the paper writing. M.M. conceived and supervised the project, interpreted data and wrote the paper. All authors participated to data discussion, reviewed the manuscript and approved its submission.

References

1. Kirchain, R.; Kimerling, L.C., *Nat. Photonics,* **2007**, *1*, 303.
2. Priolo, F.; Gregorkiewicz, T.; Galli, M.; Krauss, T.F., *Nat. Nanotechnol.,* **2014**, *9*, 19.
3. Kenyon, A. J., *Semicond. Sci. Technol.,* **2005**, *20*, R65.
4. Ramirez, J. M.; Lupi, F. F.; Jambois, O.; Berencen, Y.; Navarro-Urrios, D.; Anopchenko, A.; Marconi, A.; Prtljaga, N.; Tengattini, A.; Pavesi, L.; Colonna, J.P.; Fedeli, J. M.; Garrido, B., *Nanotechnology,* **2012**, *23*, 125203.
5. Miniscalco, W. J., *J. Light. Technol.,* **1991**, *9,* 234.
6. Polman, A., *J. Appl. Phys.,* **1997**, *82*, 1.
7. Wang, X. J.; Yuan, G.; Isshiki, H.; Kimura, T.; Zhou, Z., *J. Appl. Phys. Lett.,* **2010**, *108*, 013506.
8. Suh, K.; Shin, J. H.; Seo, S. J.; Bae, B.S., *Appl. Phys. Lett.,* **2008**, *92,* 121910.
9. Wang, X.; Zhou, P.; He, Y.; Zhou, Z., *Opt. Mater. Expr.,* **2018**, *8,* 2970.
10. Sun, H.; Yin, L.; Liu, Z.; Zheng, Y.; Fan, F.; Zhao, S.; Feng, X.; Li, Y.; Ning, C. Z., *Nat. Phot.,* **2017**, *11,* 589.
11. Miritello, M.; Lo Savio, R.; Iacona, F.; Franzò, G.; Irrera, A.; Piro, A.M.; Bongiorno, C.; Priolo, F., *Adv. Mater.,* **2007**, *1,* 1582.
12. Snoeks, E.; Kik, P.G.; Polman, A., *Opt. Mater.* **1996**, *5*, 159.
13. Miritello, M.; Cardile, P.; Lo Savio, R.; Priolo, F., *Opt. Express,* **2011**, *19*, 20761.
14. Lo Savio, R.; Miritello, M.; Cardile, P.; Priolo, F., *J. Appl. Phys.,* **2009**, *106*, 043512.
15. Evangelou, E.K.; Wiemer, C.; Fanciulli, M.; Sethu, M.; Cranton, W., *J. Appl. Phys.,* **2003**, *94*, 318.
16. Irrera, A.; Artoni, P.; Iacona, F.; Pecora, E.F.; Franzò, G.; Galli, M.; Fazio, B., *Nanotechnology,* **2012**, *23,* 075204.
17. Izeddin, I.; Timmerman, D.; Gregorkiewicz, T.; Moskalenko, A.S.; Prokofiev, A. A.; Yassievich, I.N.; Fujii, M., *Phys. Rev. B,* **2008**, *78,* 035327.
18. Cardile, P.; Miritello, M.; Priolo, F., *Appl. Phys. Lett.,* **2012**, *100,* 251913.
19. Cao, R.; Fu, T.; Cao, Y.; Ao, H.; Guo, S.; Zheng, G., *Mater. Lett.,* **2015***, 155,* 68.
20. Huang, M. N.; Ma, Y. Y.; Huang, X. Y.; Ye, S.; Zhang, Q. Y., *Spectra Acta Part A: Mol. Biomol. Spectr.* **2013**, *115,* 767.
21. Tabaza, W. A. I.; Swart, H. C.; Kroon, R.E., *J. Lumin.,* **2014** *148*, 192.
22. Peng, M.; Zhang, N.; Wondraczek, L.; Qiu, J.; Yang, Z.; Zhang, Q., *Opt. Express* **2011**, *19,* 20799.
23. Hau, T.M.; Yu, X.; Zhou, D.; Song, Z.; Yang, Z.; Wang, R.; Qiu, J., *Opt. Mater.,* **2013**, *35*, 487.
24. Bai, Z.; Sun, H.T.; Hasegawa, T.; Fujii, M.; Shimaoka, F.; Miwa, Y.; Mizuhata, M.; Hayashi, S., *Opt. Lett.,* **2010**, *35,* 1926.
25. Zheng, J. ; Zuo, Y. H.; Zhang, L.Z. ; Wang, W.; Xue, C. L.; Cheng, B.W.; Yu, J. Z.; Guo, H. Q.; Wanga, Q. M., *J. Lumin.,* **2010**, *130*, 1760.
26. Ziegler, J.; Ziegler, M.D.; Biersack, J.P.; SRIM - The stopping and range of ions in matter, Nucl. Instrum. Methods B **2010**, *268*, 1818.
27. Mayer, M.; SIMNRA 6.03 simulation program (**1997–2006**).
28. Scarangella, A.; Miritello, M.; Priolo, F., *J. Appl. Phys.,* **2014**, *116*, 123511.
29. Scarangella, A.; Reitano, R.; Priolo, F.; Miritello, M., *Mat. Sci Semicon. Proc.,* **2018** in Press.
    DOI: 10.1016/j.mssp.2018.04.017
30. Card JCPDS No. 41-1105.
31. Vetrone, F.; Boyer, J.C.; Capobianco, J.A.; Speghini, A.; Bettinelli, M., *Chem. Mater.,* **2003**, *15,* 2737.
32. Camargo, M. B.; Gomes, L.; Morato, S. P., *Opt. Mater.,* **1995**, *4*, 597.
33. Zhou, S.; Jiang, N.; Zhu, B.; Yang, H.; Ye, S.; Lakshminarayana, G.; Hao, J.; Qiu, J., *Adv. Funct. Mater.* **2008**, *18*, 1407.
34. Fujimoto Y.; Nakatsuka, M., *J. Appl. Phys.* **2001**, *40*, L279.
35. Wu, X.; Liang, Y.; Chen, R.; Liu, M.; Li, Y., *J. Mater. Sci.* **2011**, *46*, 5581.
36. Scarangella, A.; Fabbri, F.; Reitano, R.; Rossi, F.; Priolo, F.; Miritello, M., *Sci. Rep.,* **2017**, *7*, 17325.
37. Jacobsohn, L. G., et al.; *J. Appl. Phys.* **2008**, *104*, 124303.
38. Van de Craats, A. M. ; Blasse, G., *Chem. Phys. Lett.,* **1995**, *243*, 559.
39. Scarangella, A.; Reitano, R.; Franzò, G.; Priolo, F. & Miritello, M., *Appl. Phys. Lett.,* **2015**, *107*, 041908.
40. Wu, X.; Liang, Y.; Chen, R.; Liu, M.; Li, Y., *J. Mater. Sci.,* **2011**, *46*, 5581.
41. Scarangella, A.; Reitano, R.; Franzò, G.; Priolo, F.; Miritello, M., *J. Lumin.,* **2017**, *191*, 92.
42. Charbonniére, L. J.; Hildebrandt, N.; *Eur. J. Inorg. Chem.,* **2008**, 3241.
43. Daldosso et al., *Laser & Photon. Rev.,* **2009**, *3*, 508.
44. Priolo F.; et al., *J. Appl. Phys.,* **2001**, *89*, 264.
45. Pollnau, M.; Gamelin, D. R.; Lüthi, S. R.; Güdel, H. U.; Hehlen, M. P.; *Phys. Rev. B,* **2000**, *61*, 3337.
46. Capobianco, J.A.; Vetrone, F.; D'Alesio, T.; Tessari, G.; Speghini, A.; Bettinelli, M., *Phys. Chem.* **2000**, *2*, 3203.
47. Guo, H.; Qiao, Y. M., *Opt. Mater.,* **2009**, *31*, 583.
48. Weber, M. J.; Monchamp, R. R., *J. Appl. Phys.* **1973**, *44*, 5495.